Ultrawideband doublet pulse generation based on nonlinear polarization rotation of an elliptically polarized beam and its distribution over a fiber/wireless link

You Min Chang, Junsu Lee, and Ju Han Lee*

School of Electrical and Computer Engineering, University of Seoul, Seoul 130-743, Republic of Korea
** j.h.lee@ieee.org*

Abstract: Proposed herein is an alternative photonic scheme for the generation of a doublet UWB pulse, which is based on the nonlinear polarization rotation of an elliptically polarized probe beam. The proposed scheme is a modified optical-fiber Kerr shutter that uses an elliptically polarized probe beam together with a linearly polarized control beam. Through theoretical analysis, it was shown that the optical-fiber-based Kerr shutter is capable of producing an ideal transfer function for the successful conversion of input Gaussian pulses into doublet pulses under special elliptical polarization states of the probe beam. An experimental verification was subsequently carried out to verify the working principle. Finally, the system performance of the generated UWB doublet pulses was assessed by propagating them over a 25-km-long standard single-mode fiber link, followed by wireless transmission. Error-free transmission was successfully achieved.

OCIS codes: (060.4080) Modulation; (060.5625) Radio frequency photonics; (350.4010) Microwaves; (060.4370) Nonlinear optics, fibers.

References and links

1. D. Porcino, and W. Hirt, "Ultra-wideband radio technology: Potential and challenges ahead," IEEE Commun. Mag. **41**(7), 66–74 (2003).
2. Fed. Commun. Commission, Revision of Part 15 of the Commission's Rules Regarding Ultra-Wideband Transmission Systems, Tech. Rep. ET-Docket 98–153, FCC02–48, Apr. (2002).
3. M. Z. Win, and R. A. Scholtz, "Ultra-wide bandwidth time-hopping spread-spectrum impulse radio for wireless multiple-access communications," IEEE Trans. Commun. **48**(4), 679–689 (2000).
4. R. Llorente, T. Alves, M. Morant, M. Beltran, J. Perez, A. Cartaxo, and J. Marti, "Ultra-Wideband Radio Signals Distribution in FTTH Networks," IEEE Photon. Technol. Lett. **20**(11), 945–947 (2008).
5. Q. Wang, and J. Yao, "UWB doublet generation using a nonlinearly-biased electro-optic intensity modulator," Electron. Lett. **42**(22), 1304–1305 (2006).
6. V. Torres-Company, K. Prince, and I. T. Monroy, "Fiber transmission and generation of ultrawideband pulses by direct current modulation of semiconductor lasers and chirp-to-intensity conversion," Opt. Lett. **33**(3), 222–224 (2008).
7. J. Li, K. Xu, S. Fu, J. Wu, J. Lin, M. Tang, and P. Shum, "Ultra-wideband pulse generation with flexible pulse shape and polarity control using a Sagnac-interferometer-based intensity modulator," Opt. Express **15**(26), 18156–18161 (2007).
8. F. Zeng, and J. Yao, "Ultrawideband impulse radio signal generation using a high-speed electrooptic phase modulator and a fiber-Bragg-grating-based frequency discriminator," IEEE Photon. Technol. Lett. **18**(19), 2062–2064 (2006).
9. Q. Wang, and J. Yao, "An electrically switchable optical ultrawideband pulse generator," J. Lightwave Technol. **25**(11), 3626–3633 (2007).
10. T.-H. Wu, J. P. Wu, and Y.-J. Chiu, "Novel ultra-wideband (UWB) photonic generation through photodetection and cross-absorption modulation in a single electroabsorption modulator," Opt. Express **18**(4), 3379–3384 (2010).
11. Q. Wang, F. Zeng, S. Blais, and J. Yao, "Optical ultrawideband monocycle pulse generation based on cross-gain modulation in a semiconductor optical amplifier," Opt. Lett. **31**(21), 3083–3085 (2006).

#128663 - $15.00 USD Received 20 May 2010; revised 22 Jul 2010; accepted 9 Aug 2010; published 3 Sep 2010

12. J. Li, B. P.-P. Kuo, and K. K.-Y. Wong, "Ultra-wideband pulse generation and based on cross-gain modulation in fiber optical parametric amplifier," IEEE Photon. Technol. Lett. **21**(4), 212–214 (2009).
13. H. Huang, K. Xu, J. Li, J. Wu, X. Hong, and J. Lin, "UWB pulse generation and distribution using a NOLM based optical switch," J. Lightwave Technol. **26**(15), 2635–2640 (2008).
14. F. Zeng, Q. Wang, and J. Yao, "All-optical UWB impulse generation based on cross-phase modulation and frequency discriminator," Electron. Lett. **43**(2), 119–122 (2007).
15. G. P. Agrawal, *Nonlinear Fiber Optics*, 4th ed. (Academic Press, San Diego, CA, 2007).
16. J. Suzuki, K. Taira, Y. Fukuchi, Y. Ozeki, T. Tanemura, and K. Kikuchi, "All-optical time-division add-drop multiplexer using optical fibre Kerr shutter," Electron. Lett. **40**(7), 445–446 (2004).
17. J. H. Lee, T. Nagashima, T. Hasegawa, S. Ohara, N. Sugimoto, and K. Kikuchi, "Wide-band tunable wavelength conversion of 10-Gb/s nonreturn-to-zero signal using cross-phase-Modulation-induced polarization rotation in 1-m bismuth oxide-based nonlinear optical fiber," IEEE Photon. Technol. Lett. **18**(1), 298–300 (2006).
18. K. Kitayama, Y. Kimura, and S. Seikai, "Fiber-optic logic gate," Appl. Phys. Lett. **46**(4), 317–319 (1985).
19. A. Yariv, and P. Yeh, *Photonics: Optical Electronics in Modern Communications* (Oxford Univ. Press, New York, 2007).
20. C. Wu, and N. K. Dutta, "High-repetition-rate optical pulse generation using a rational harmonic mode-locked fiber laser," IEEE J. Quantum Electron. **36**(2), 145–150 (2000).
21. R. H. Stolen, J. Botineau, and A. Ashkin, "Intensity discrimination of optical pulses with birefringent fibers," Opt. Lett. **7**(10), 512–514 (1982).
22. T. Tanemura, and K. Kikuchi, "Circular-birefringence fiber for nonlinear optical signal processing," J. Lightwave Technol. **24**(11), 4108–4119 (2006).
23. M. Abtahi, J. Magné, M. Mirshafiei, L. A. Rusch, and S. LaRochelle, "Generation of power-efficient FCC-compliant UWB waveforms using FBGs: analysis and experiment," J. Lightwave Technol. **26**(5), 628–635 (2008).
24. Y. M. Chang, J. S. Lee, D. Koh, H. Chung, and J. H. Lee, ""Ultra-wideband doublet pulse generation based on semiconductor electroabsorption modulator and its distribution over a fiber/wireless link", To be published in J," Opt. Commun. Netw. **2**(8), 600–608 (2010).
25. T. B. Gibbon, X. Yu, and I. T. Monroy, "Photonic ultra-wideband 781.25-Mb/s signal generation and transmission incorporating digital signal processing detection," IEEE Photon. Technol. Lett. **21**(15), 1060–1062 (2009).
26. H. Shams, A. Kaszubowska-Anandarajah, P. Perry, P. Anandarajah, and L. P. Barry, "Electro-optical generation and distribution of ultrawideband signals based on the gain switching technique," J. Opt. Commun. Netw. **2**(3), 122–130 (2010).

1. Introduction

Ultrawideband (UWB) radio technology has been receiving much attention of late as a highly promising solution for future high-capacity wireless personal-area networks (PANs) due to its various benefits, such as low power consumption, high data capacity, and multipath fading immunity [1]. The UWB signal transmission is realized by spreading a small amount of radiated radio frequency power across a very wide frequency band relative to its center frequency. The U.S. Federal Communications Commission (FCC) Report and Order issued in 2002 defines the UWB signal as any signal that possesses a spectral bandwidth of more than 500 MHz in the 3.1~10.6 GHz band, with a spectral power density lower than −41.3 dBm/MHz [2]. The commonly used UWB transmission systems are implemented based on the impulse radio UWB (IR-UWB) or orthogonal-frequency-division-multiplexing UWB (OFDM-UWB) schemes. The IR-UWB technology, which transmits data via ultrashort temporal pulses, is an attractive technique due to its carrier-free modulation and low power consumption, and because it does not require the use of frequency mixers [3].

Although the IR-UWB technology can provide a variety of technical advantages, such as reduced multipath fading, broad bandwidth, and increased operational security, it has the fundamental limitation of low spectral-power density, which allows it to cover only a short signal transmission distance of less than tens of meters. As a potential solution, the use of UWB-over-fiber technology, with which the generation, modulation, and distribution of UWB signals are implemented in the optical domain, was proposed, and its feasibility has been successfully demonstrated [4]. Although UWB signals can have step and Gaussian waveforms, the commonly employed waveforms are monocycle- and doublet-shaped as these waveforms possess reduced low-frequency components.

#128663 - $15.00 USD Received 20 May 2010; revised 22 Jul 2010; accepted 9 Aug 2010; published 3 Sep 2010

A number of optical schemes have been proposed for the generation of monocycle or doublet UWB pulses, such as waveform transformation from a Gaussian pulse to a doublet pulse using a nonlinearly biased electro-optic modulator [5], monocycle pulse generation through the direct-current modulation of semiconductor lasers followed by chirp-to-intensity conversion [6], Sagnac-interferometer-based intensity modulation for both monocycle and doublet pulse generation [7], electro-optic phase modulation (PM) followed by PM-to-intensity conversion with the use of a frequency discriminator or a chromatic dispersive element [8], polarization modulation and subsequent different time delays [9], the use of the cross-absorption modulation effect in an electroabsorption modulator [10] and the cross-gain modulation effect in a semiconductor optical amplifier (SOA) [11] for the generation of monocycle pulses, and the use of the cross-gain modulation (XGM) effect in a fiber optic parametric amplifier [12]. A nonlinear optical-loop mirror based on optical fiber has also been used for the generation of monocycle or doublet pulses [13].

These techniques can be roughly classified as electro-optic conversion-based and all-optical schemes. The electro-optic conversion-based schemes use an electrical Gaussian pulse as an input seed signal, and electro-optic converters are used as signal-processing units [5,6,8–10]. On the other hand, the all-optical schemes use a short optical pulse as an input seed, and nonlinear optical media, such as semiconductor optical amplifiers and nonlinear optical fibers, as signal-processing units [7,11–13]. One benefit of all-optical schemes is no need for extra electro-optic conversion that makes the whole system complicated. In other words, they not require high speed electrical pulse generators and high speed electro-optic modulators, since the UWB pulse generation is performed in the optical domain [14].

High-quality IR-UWB signals have been successfully achieved through the foregoing schemes, but there is still a huge demand for the expansion of the technological bases for alternative UWB signal generation and distribution schemes.

In this study, an alternative photonic scheme for the generation of doublet UWB pulses was proposed, and its operating principle was experimentally verified. The proposed scheme, which is an all-optical one with an all-fiber-integrated structure, is based on the optical-fiber-based Kerr shutter configuration using the nonlinear-polarization-rotation (NPR) principle [15]. The conventional optical-fiber-based Kerr shutters, which use both linearly polarized control and probe beams, have been widely used for nonlinear signal processing, such as data demultiplexing in high-speed optical-time-domain-multiplexing (OTDM) systems [16], wavelength conversion [17], and logic gates [18].

Unlike the commonly used Kerr shutter configurations, the proposed scheme uses an elliptically polarized probe beam together with a linearly polarized control beam. Through theoretical analysis, the optical-fiber-based Kerr shutter was shown to be capable of producing an ideal transfer function for the successful conversion of input Gaussian pulses into doublet pulses under special polarization conditions of the input beams. Note that the use of elliptically polarized probe beams rather than linearly polarized ones in implementing optical-fiber Kerr shutters has not been reported so far. An experimental demonstration was subsequently carried out to verify the working principle of the proposed scheme. Finally, the system performance of the generated UWB doublet pulses was evaluated by propagating them over a 25-km-long standard single-mode fiber (SMF) link, followed by wireless transmission. Error-free transmission was successfully achieved.

Compared to other all-optical UWB pulse generation schemes our proposed scheme has a noticeable advantage that the produced doublet pulse has a single operating wavelength. It should be noted that most of the all-optical UWB pulse generation schemes were based on the simultaneous generation of multiple Gaussian pulses with opposite polarities followed by the time-delayed temporal overlap [7,11–13]. In these schemes the multiple Gaussian pulses must have different operating wavelengths; otherwise, the temporal overlap induces significant coherent noise at the output signal. Such UWB optical pulses thus suffer from optical fiber dispersion-induced transmission distance limitation. However, the optical doublet pulses

#128663 - $15.00 USD Received 20 May 2010; revised 22 Jul 2010; accepted 9 Aug 2010; published 3 Sep 2010

produced from our proposed scheme does not suffer from the fiber dispersion-induced limitation, since it is a single wavelength signal.

2. Operating principle

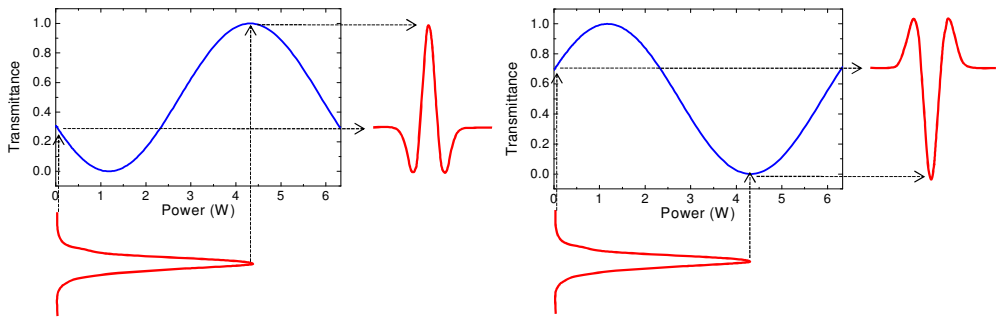

(a) (b)

Fig. 1. (a) Ideal transfer function for the waveform conversion from Gaussian input pulses to doublet pulses. (b) Ideal transfer function for inverted doublet pulse generation.

To produce doublet optical pulses from input Gaussian-shaped optical pulses, an all-optical pulse-shaping device that has transfer functions, as shown in Fig. 1(a) and (b), is essentially required. These kinds of transfer function are different from the $\sin^2()$- or $\cos^2()$-shaped ones shown in Fig. 2(b), which can be obtained from the conventional linear-polarization-based Kerr shutter configurations [15] shown in Fig. 2(a). It should be noted that the required transfer functions of Fig. 1 are phase-shifted versions of the ones in Fig. 2. In this section, simple mathematical analysis is performed to show that the transfer functions of Fig. 1 can be readily obtained from the Kerr shutter configuration if a control beam has a linear state of polarization (SOP) and a probe beam with a special elliptical SOP.

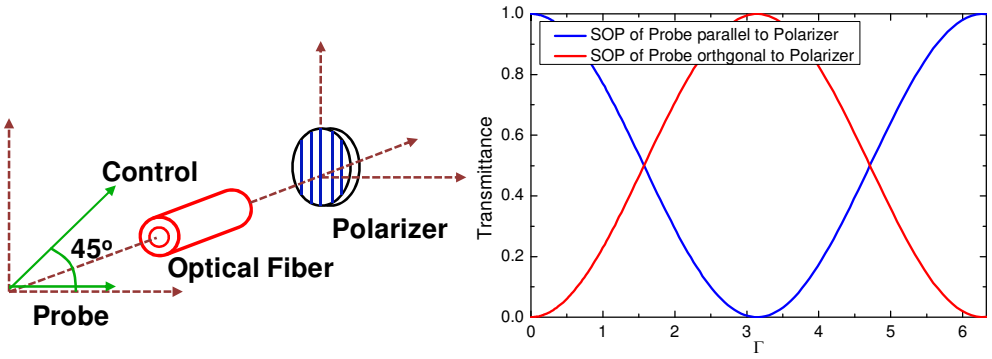

(a) (b)

Fig. 2. (a) Commonly used Kerr shutter configuration and (b) its transfer functions depending on the SOPs of the probe beam and the polarizer.

For a better understanding of the working principle, let an analytical formula of the Kerr shutter transfer function be derived for the arbitrary SOPs of the probe beam. When NPR occurs in an optical fiber, the fiber acts as a birefringent-phase plate. The optical-fiber-based Kerr shutter system can thus be modeled by using the Jones matrix method. The Jones vectors of the probe beams with arbitrary SOPs can be expressed using a righthand elliptical (RHE) SOP or a lefthand elliptical (LHE) SOP [19].

#128663 - $15.00 USD Received 20 May 2010; revised 22 Jul 2010; accepted 9 Aug 2010; published 3 Sep 2010

$$\mathbf{E}_{\mathbf{probe}} = \begin{bmatrix} a\cos\varphi + ib\sin\varphi \\ a\sin\varphi - ib\cos\varphi \end{bmatrix} \text{ for RHE } \begin{bmatrix} a\cos\varphi - ib\sin\varphi \\ a\sin\varphi + ib\cos\varphi \end{bmatrix} \text{ for LHE} \tag{1}$$

where φ is the angle between the longer axis of the polarization ellipsoid and the x-axis, and a and b are coefficients that determine the degree of ellipticity and that have the relation of $\sqrt{a^2 + b^2} = 1$. Here, $a/b = 0$ or $a/b = \infty$ pertains to linear polarization, and $a/b = 1$ to circular polarization. The birefringent plate of the optical fiber can be expressed as follows [15].

$$\mathbf{M} = \begin{bmatrix} e^{-i\Gamma/2}\cos^2\psi + e^{i\Gamma/2}\sin^2\psi & -i\sin(\Gamma/2)\sin(2\psi) \\ -i\sin(\Gamma/2)\sin(2\psi) & e^{-i\Gamma/2}\sin^2\psi + e^{i\Gamma/2}\cos^2\psi \end{bmatrix} \tag{2}$$

where ψ is the angle between the slow axis of the birefringent plate and the x-axis, and Γ is the phase retardation between the slow and fast axes, which is given by the following relation.

$$\Gamma = \frac{2\pi}{\lambda}(n_s - n_f)L_{eff} \tag{3}$$

where n_s and n_f are refractive indices for the slow and fast axes, respectively; λ is the beam wavelength; and L_{eff} is the effective length of the nonlinear fiber. The SOP of a linearly polarized control beam decides the slow axis of the nonlinear fiber if the self-phase modulation (SPM) is neglected [14].

$$n_s = n_{s,linear} + 2n_2\left|E_C{}^2\right| \tag{4}$$

$$n_f = n_{f,linear} + 2n_2 B\left|E_C{}^2\right| \tag{5}$$

where $n_{s,linear}$ and $n_{f,linear}$ are the linear parts of the refractive indices for the slow and fast axes, respectively; n_2 is the nonlinear index coefficient; and E_C is the peak power of the control beam. If $\chi^{(3)}$ is originated from a purely electronic response, then $B = 1/3$ [14]. Assuming $n_{s,linear} = n_{f,linear}$ for isotropic fiber, the phase retardation Γ can be expressed as

$$\Gamma = \frac{8}{3}\frac{\pi L_{eff}}{\lambda}n_2\left|\mathrm{E}_C\right|^2 \tag{6}$$

The polarizer has the following vector expression.

$$\mathbf{P} = \begin{bmatrix} 1 & 0 \\ 0 & 0 \end{bmatrix} \text{ aligned to x-axis, } \begin{bmatrix} 0 & 0 \\ 0 & 1 \end{bmatrix} \text{ aligned to y-axis} \tag{7}$$

Then, the output beam has the following form.

$$\mathbf{E}_{\mathbf{Out}} = \mathbf{PME}_{\mathbf{probe}} \tag{8}$$

The transfer function is given by

$$T = \left|\mathbf{E}_{\mathbf{out}}\right|^2 \Big/ \left|\mathbf{E}_{\mathbf{probe}}\right|^2 \tag{9}$$

Using Eqs. (8) and (9), four different combinations of the SOPs of the probe beam and polarizer were analyzed in terms of the transfer function. It was shown that the ideal transfer functions of Fig. 1 for UWB doublet pulse generation can be obtained by using elliptically polarized probe beams.

#128663 - $15.00 USD Received 20 May 2010; revised 22 Jul 2010; accepted 9 Aug 2010; published 3 Sep 2010

2.1 Probe beam: RHE SOP; Polarizer: x-axis

Consider a case where the probe has an RHE SOP and where the polarizer is aligned to the x-axis, as shown in Fig. 3(a). For the sake of easy calculation, let it be assumed that $\varphi = 0^o$ and $\psi = 45^o$. Using Eqs. (8) and (9), the transmittance T can be calculated as follows:

$$T = a^2 \cos^2(\Gamma/2) + b^2 \sin^2(\Gamma/2) - 2ab\cos(\Gamma/2)\sin(\Gamma/2) \qquad (10)$$

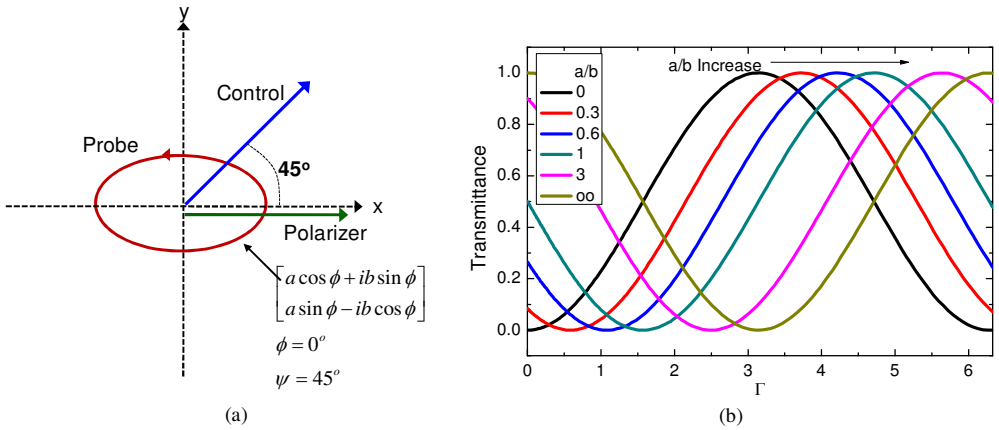

Fig. 3. (a) Polarization arrangement: probe beam, RHE SOP; polarizer, x-axis. (b) Calculated transmittance as a function of the ellipticity ratio a/b of the probe beam.

Figure 3(b) shows the calculated transmittance as a function of the ellipticity ratio a/b. It is evident from the graph that the minimum transmission point moves to the righthand side as the a/b ratio increases. From Fig. 2 it can be easily inferred that the ideal transfer function, like Fig. 1(a), which is suitable for doublet pulse generation, can be readily produced by controlling the ellipticity ratio a/b of the probe beam. $a/b = 0.66$ was found to lead to the ideal transfer function of Fig. 1(a).

2.2 Probe beam: RHE SOP; Polarizer: y-axis

In the case where a probe beam with an RHE SOP is used together with a polarizer aligned to the y-axis, as shown in Fig. 4(a), the transmittance T can be calculated as follows.

$$T = a^2 \sin^2(\Gamma/2) + b^2 \cos^2(\Gamma/2) + 2ab\cos(\Gamma/2)\sin(\Gamma/2) \qquad (11)$$

Figure 4(b) shows the calculated transmittance as a function of the ellipticity ratio a/b. Interestingly, it can be seen that the transfer function of Fig. 1(b), which is suitable for the generation of inverted doublet pulses, can be obtained by controlling the ellipticity ratio a/b. $a/b = 0.66$ was found to lead to the ideal transfer function of Fig. 1(b).

#128663 - $15.00 USD Received 20 May 2010; revised 22 Jul 2010; accepted 9 Aug 2010; published 3 Sep 2010

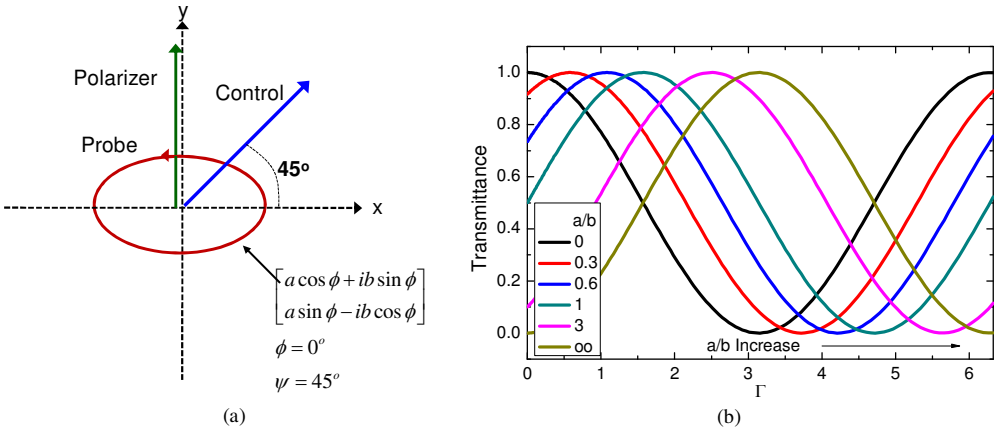

Fig. 4. (a) Polarization arrangement: probe beam, RHE SOP; polarizer: y-axis. (b) Calculated transmittance as a function of the ellipticity ratio a/b of the probe beam.

2.3 Probe beam: LHE SOP; Polarizer: x-axis

In the case where a probe beam with an LHE SOP is used together with a polarizer aligned to the x-axis, as shown in Fig. 5(a), the transmittance T can be given by

$$T = a^2\cos^2(\Gamma/2) + b^2\sin^2(\Gamma/2) + 2ab\cos(\Gamma/2)\sin(\Gamma/2) \qquad (12)$$

From Fig. 5(b), $a/b = 1.5$ was found to result in the ideal transfer function of Fig. 1(b) for inverted doublet pulse generation.

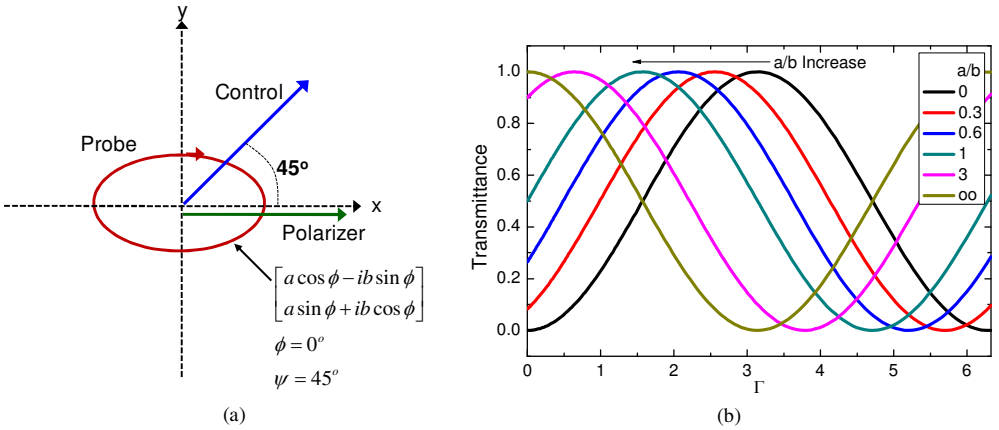

Fig. 5. (a) Polarization arrangement: probe beam, LHE SOP; polarizer, x-axis. (b) Calculated transmittance as a function of the ellipticity ratio a/b of the probe beam.

2.4 Probe beam: LHE SOP; Polarizer: y-axis

In the case where a probe beam with an LHE SOP is used together with a polarizer aligned to the y-axis, the transmittance T can be given by

$$T = a^2\sin^2(\Gamma/2) + b^2\cos^2(\Gamma/2) - 2ab\cos(\Gamma/2)\sin(\Gamma/2) \qquad (13)$$

From Fig. 6(b), $a/b = 1.5$ was found to result in the ideal transfer function of Fig. 1(a) for doublet pulse generation.

#128663 - $15.00 USD Received 20 May 2010; revised 22 Jul 2010; accepted 9 Aug 2010; published 3 Sep 2010

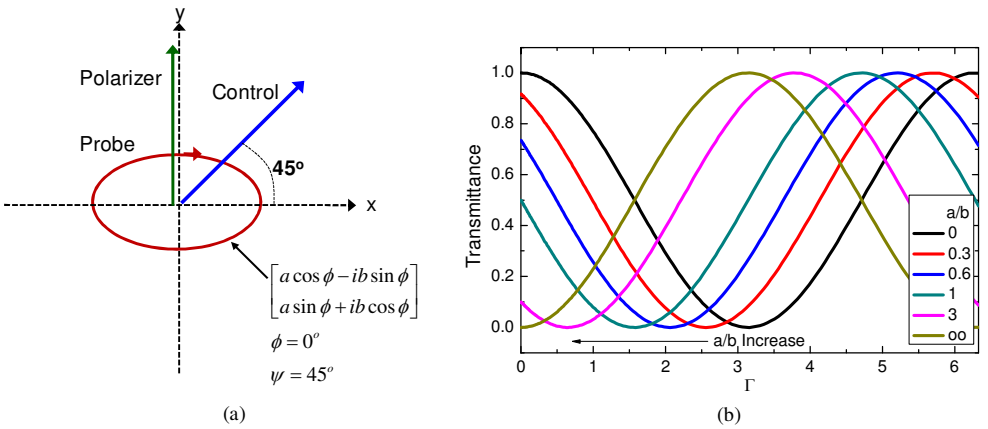

Fig. 6. (a) Polarization arrangement: probe beam, LHE SOP; polarizer, y-axis. (b) Calculated transmittance as a function of the ellipticity ratio a/b of the probe beam.

3. Experimental verification of the proposed doublet pulse generation principle

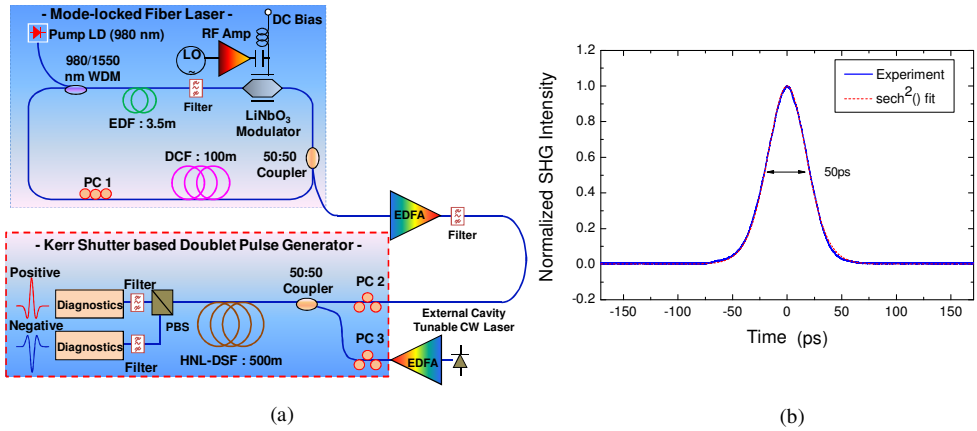

Fig. 7. (a) Experimental configuration to verify the proposed doublet pulse generation principle. (b) Measured autocorrelation trace of the actively-mode-locked fiber laser output pulse, which was used as an input pulse.

To verify the proposed doublet pulse generation principle, an experimental setup was constructed, as shown in Fig. 7(a). First, an actively-mode-locked fiber laser [20] that can generate ~50-ps-wide soliton pulses, as shown in the measured autocorrelation trace in Fig. 2(b), was built. Note that all the experiments in this work were performed with the soliton pulses since the mode-locked fiber laser generated soliton pulses rather than Gaussian pulses. The mode-locked fiber laser was composed of a 3.5-m-long erbium-doped fiber (EDF), a 980-nm pump laser diode, a 980/1550-nm-wavelength division multiplexer, a $LiNbO_3$ modulator, a 50:50 coupler, a 100-m-long dispersion-compensating fiber, and a polarization controller (PC). By changing the RF frequency of the sinusoidal electrical signal coupled to the modulator, the repetition rate of the output optical pulses could be changed from ~300 MHz to ~3 GHz. For this particular experiment, the mode-locked laser was operated at 623 MHz. The generated soliton pulses were used as a control beam for a Kerr shutter. The soliton control beam and a continuous-wave (CW) probe beam from an external-cavity tunable laser were amplified using erbium-doped fiber amplifiers (EDFAs) and were then combined using a 50:50 coupler. The SOP of each beam was adjusted by using a PC in front of the 50:50 coupler. They were subsequently launched into a 500-m-long highly nonlinear dispersion-

#128663 - $15.00 USD Received 20 May 2010; revised 22 Jul 2010; accepted 9 Aug 2010; published 3 Sep 2010

shifted fiber (HNL-DSF). The power levels of the control and probe beams that were coupled into the HNL-DSF were measured to be ~14 dBm and 3.6 dBm, respectively, and their operating wavelengths were 1538.1 nm and 1542.1 nm, each. The nonlinear parameter and zero dispersion wavelength of the HNL-DSF were ~28 W/km and ~1552 nm, respectively. A polarization beam splitter rather than a polarizer was connected to the output end of the HNL-DSF to monitor the outputs of the x- and y-axes at the same time. A 1-nm band pass filter was used after the PBS to filter out the residual control beam components.

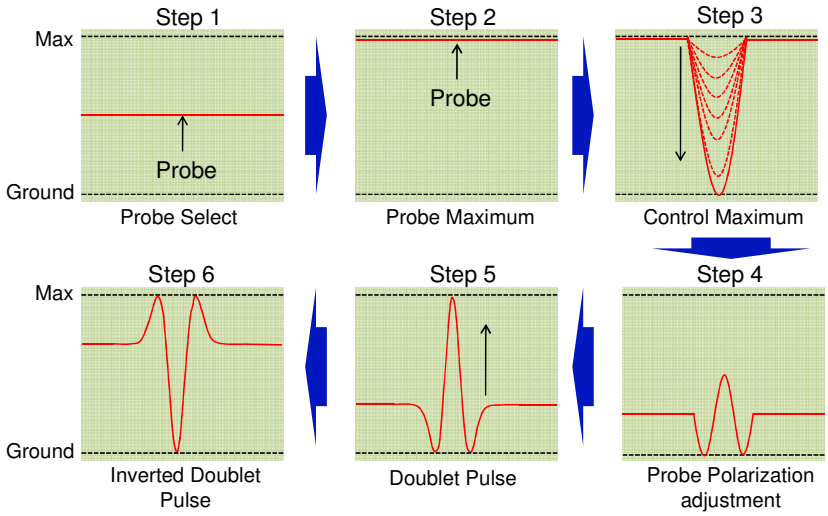

Fig. 8. Procedure for the adjustment of the SOPs of the control and probe beams.

One key issue in successfully carrying out this proof-of-principle experiment was how to precisely control the SOPs of the control and probe beams. In particular, the most difficult task was to ensure that the elliptical SOPs of the probe beams would have specific ellipticity ratios of a/b. For this purpose, a novel procedure was devised involving the real-time measurement of the output pulse from the Kerr shutter, as follows:

Step 1: Select one of the two output ports from the PBS and denote it as the x-axis. Then the other automatically becomes the y-axis.

Step 2: Launch the CW probe beam into the Kerr shutter and adjust its SOP with the use of a PC to ensure the maximum output power at the x-axis output. The SOP of the probe beam is now parallel to the x-axis of the PBS.

Step 3: Launch the control beam with medium-level optical power into the Kerr shutter and adjust its SOP with the use of a PC to ensure the largest negative pulse appearing at the probe beam, as shown in Fig. 8. This step ensures that the control beam has linear polarization with a 45° angle relative to the x-axis of the PBS. Note that the control beam cannot otherwise induce the largest negative pulse.

Step 4: Adjust the SOP of the probe beam with the use of a PC to produce a doublet-like pulse, as shown in Fig. 8. The relative level of the background CW component must be adjusted to 30% of the original CW probe level. This step ensures that the probe beam has an RHE SOP with $a/b = 0.66$.

Step 5: Increase the power of the control pulse to make the doublet-like pulse evolve into a perfect doublet pulse.

#128663 - $15.00 USD Received 20 May 2010; revised 22 Jul 2010; accepted 9 Aug 2010; published 3 Sep 2010

Step 6: Check the output pulse at the y-axis output from the PBS to ensure that the pulse has an inverted doublet pulse shape.

A few iterative PC adjustments were made to obtain the desired doublet or inverted-doublet pulses as the non-polarization-maintaining (PM) HNL-DSF that was used had a degree of polarization instability.

Figure 9 shows the experimentally measured transfer functions at the x- and y-axis outputs of the PBS together with the theoretically calculated ones. Even if the experimental transfer functions were in good agreement with the theoretical ones at low control power regimes, there was some degree of discrepancy at the higher control power regimes. This phenomenon is believed to be due to the NPR efficiency reduction caused by the SPM-induced NPR of the control beam itself [21] or by the random distribution of the birefringence of the non-PM HNL-DSF that was used [22].

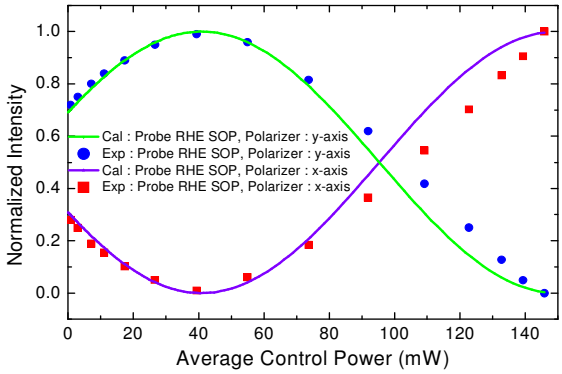

Fig. 9. Experimentally measured and theoretically calculated transfer functions.

Figure 10 shows the measured oscilloscope trace of the UWB doublet pulse produced from the x-axis output of the PBS, together with its corresponding measured RF spectrum. It is evident from the graph that the desired UWB doublet pulse was readily achieved. The full width at half maximum (FWHM) of the generated pulse was ~47 ps, and the interval of the two negative peaks at both sides was ~90 ps. The center frequency and 10 dB bandwidth of the generated UWB doublet pulse were estimated to be ~9 and ~10 GHz, respectively. Accordingly, the fractional bandwidth was ~111%. To make the RF spectrum of the UWB signal meet the FCC requirement we have properly adjusted the optical power levels of the control and probe beams [23].

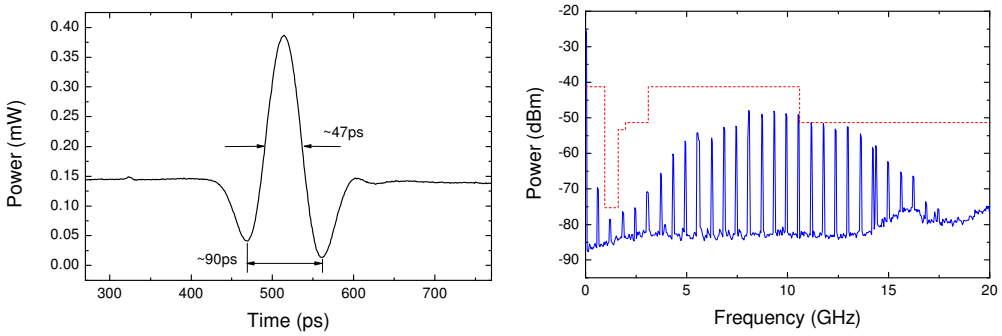

(a) (b)

Fig. 10. (a) Measured oscilloscope trace and (b) measured RF spectrum of the generated doublet pulse. The FCC mask is plotted by a dotted line.

#128663 - $15.00 USD Received 20 May 2010; revised 22 Jul 2010; accepted 9 Aug 2010; published 3 Sep 2010

On the other hand, the oscilloscope trace and RF spectrum of the inverted-UWB-doublet pulse produced from the y-axis output of the PBS are shown in Fig. 11. The FWHM of the generated pulse and the interval of the two negative peaks at both sides were ~51 and ~100 ps, respectively. The center frequency and 10 dB bandwidth of the generated UWB doublet pulse were estimated to be ~8.1 and ~8.95 GHz, respectively. Accordingly, the fractional bandwidth was ~111%. A noticeable performance difference between the produced UWB doublet and inverted-doublet pulses was observed despite the fact that the same Kerr shutter was used. This is believed to be due to the polarization uncertainty of the probe beam. In other words, it was slightly difficult to ensure in practice that the probe beam has a perfect RHE SOP with an ellipticity ratio of $a/b = 0.66$.

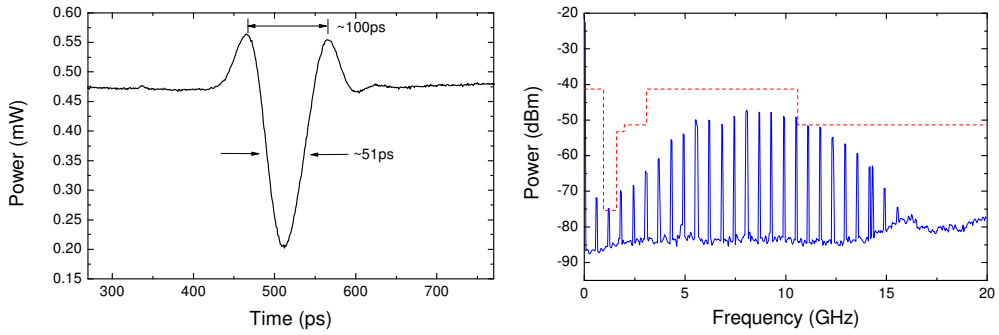

(a) (b)

Fig. 11. (a) Measured oscilloscope trace and (b) measured RF spectrum of the generated inverted-doublet pulse.

4. System performance assessment of the UWB doublet pulse generated over fiber/wireless transmission link

4.1 System Setup

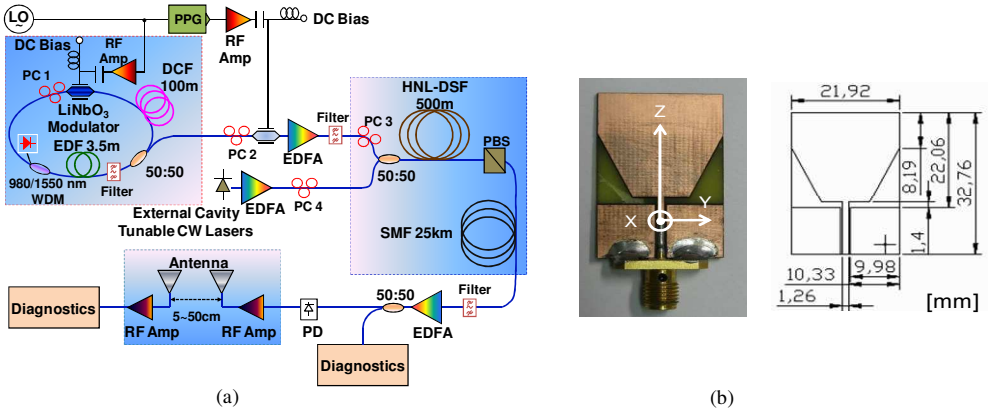

(a) (b)

Fig. 12. (a) Experimental configuration for 1.25Gbit/s UWB doublet pulse transmission over a fiber/wireless link. (b) A real photo and a schematic diagram of the design of the antenna that was used in the experiment.

To assess the system performance of the generated UWB pulses, a signal transmission experiment with a data rate of 1.25 Gbit/s was subsequently performed over a 25-km-long standard SMF link, followed by a 5 ~50-cm wireless link, using the setup in Fig. 12(a). For this experiment, soliton optical pulses were first produced at a repetition rate of 1.25 GHz. They were then on- and off-keying-modulated to provide a 2^7-1 pseudorandom bit sequence

#128663 - $15.00 USD Received 20 May 2010; revised 22 Jul 2010; accepted 9 Aug 2010; published 3 Sep 2010

(PRBS) using a $LiNbO_3$ modulator. The modulated soliton pulses were amplified and used as a control beam for the Kerr shutter, whereas a CW beam from an external-cavity tunable laser was used as a probe. The PRBS-modulated doublet optical pulses generated from the Kerr shutter were then propagated over a 25-km-long standard SMF link. After 25-km fiber transmission, the 1.25 Gbit/s PRBS doublet pulse stream was optically amplified through an EDFA and then coupled into a 15GHz photodetector to convert the optical doublet pulse into an electrical one. The electrical UWB doublet pulse was amplified using an inverting RF amplifier, and was fed into a transmitter antenna. A receiver antenna was set to be 5 ~50 cm away from the transmitter antenna. The output signal from the receiver antenna was amplified by a low-noise amplifier (LNA) and detected by a digital-communication analyzer or an error detector.

An omnidirectional antenna, which was designed based on the coplanar-waveguide (CPW) UWB antenna principle, was used. The peak gain varied from 5 to 10 dBi within the 3~10GHz UWB spectrum. Further details on the antennas that were used are fully described in Ref [24]. The wireless-transmission experiment was carried out under open-air conditions, without electromagnetic-interference-noise shielding.

4.2 Transmission over a 25-km SMF link

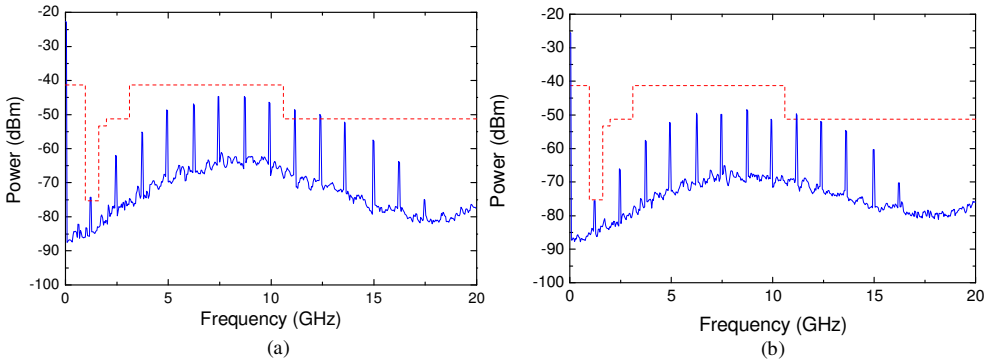

Fig. 13. Measured RF spectra of the 1.25Gbit/s PRBS UWB doublet pulse stream. (a) Back-to-back and (b) 25-km transmission.

The measured electrical spectra of the PRBS doublet data stream after 25-km transmission are shown in Fig. 13 together with the back-to-back spectrum. The original RF spectral components were well maintained after 25-km transmission even if the background noise had been increased. To quantify the system, impact BER and eye diagram measurements were performed, as shown in Fig. 14. Error-free performance could be obtained, albeit with a power penalty of ~2 dB relative to the back-to-back measurement. Note that the eye patterns shown in Fig. 14(a) exhibit inverted-doublet pulse patterns due to the use of an inverting RF amplifier right before the use of the transmitter antenna. For the BER measurement we used a p-i-n TIA receiver without incorporating an optical preamplifier [25]. Note that we did not employ a photo-receiver incorporating an optical preamplifier, which is commonly used to measure BER in fiber-optic communication systems. This was because we were not sure whether such a receiver could be used in UWB-based fiber/wireless transmission systems, even though the sort of photo-receiver had been employed to measure BER of a UWB signal transmitted over a fiber link in Ref [26].

#128663 - $15.00 USD Received 20 May 2010; revised 22 Jul 2010; accepted 9 Aug 2010; published 3 Sep 2010

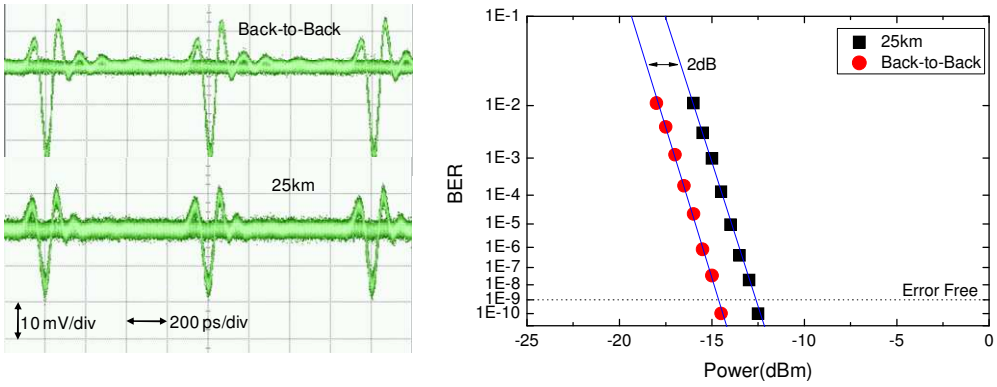

(a) (b)

Fig. 14. (a) Measured eye diagrams. (b) Measured BER vs. received optical power after 25-km fiber transmission.

4.3 Wireless Transmission after 25-km fiber transmission

Finally, the wireless-transmission performance of the PRBS doublet data stream transmitted over a 25-km SMF link was assessed using the eye diagram and via BER measurements together with RF spectrum measurement. Figure 15(a) shows the RF spectrum of the PRBS doublet data stream, which was measured at the point between the transmitter antenna and the transmitter RF amplifier, whereas Fig. 15(b) illustrates the data stream spectrum after the receiver RF amplifier cascaded to the receiver antenna. Note that the transmitter antenna response was not included in Fig. 15(a). Considering the transmitter antenna response the RF spectrum of Fig. 15(a) meets the FCC regulation. The power spectral density and total power of the UWB wireless signal from the transmitter antenna was adjusted to meet the FCC regulation.

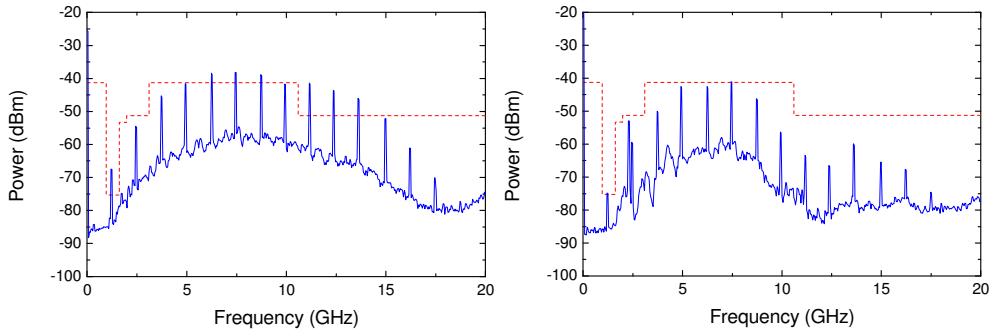

(a) (b)

Fig. 15. RF spectra of the PRBS doublet data stream measured at the point: (a) between the transmitter antenna and the transmitter RF amplifier and (b) after the receiver RF amplifier cascaded to the receiver antenna.

After transmission, the RF spectral components located at the frequency band higher than ~10 GHz substantially disappeared due to the antenna response, but sufficient RF spectral components were still quite well maintained over a broad frequency range. Figure 16(a) shows the measured BER as a function of wireless transmission distance. Considering forward error correction (FEC) limit (2 x 10^{-3}) the maximum wireless transmission distance of the PRBS doublet data stream after 25-km fiber transmission was found to be ~45 cm. Figure 16(b) shows the measured eye diagram of the wireless-transmitted pulses at BER = ~10^{-5} after 30-cm wireless transmission. A clean and open eye was evidently observed, and this means

#128663 - $15.00 USD Received 20 May 2010; revised 22 Jul 2010; accepted 9 Aug 2010; published 3 Sep 2010

that the proposed fiber/wireless-transmission system works well at a 1.25 Gbit/s data rate. The wireless-transmission distance was limited to ~45 cm due to the various wireless noise components and low antenna gain. A significant improvement in the receiver design is required to increase the wireless-transmission distance.

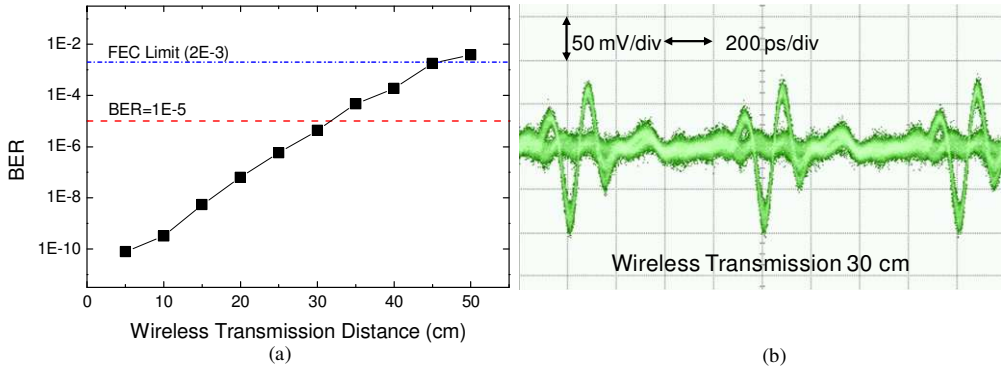

Fig. 16. , (a) Measured BER v.s. wireless transmission distance. (b) Eye diagram at BER = ~10^{-5} after 30-cm wireless transmission. The wireless signal transmission of the UWB doublet signal was carried out after 25-km transmission over a SMF link.

5. Conclusion

Demonstrated herein was an all-optical UWB doublet pulse generation scheme based on an optical-fiber Kerr shutter, using the combination of an elliptically polarized CW probe beam and a linearly polarized control pulse beam. Through both theoretical analysis and a proof-of-principle demonstration experiment, it was shown that the successful conversion of input Gaussian pulses into doublet pulses can be achieved by using the proposed scheme. The system performance of the generated UWB doublet pulses was also assessed by propagating them over a 25-km-long standard SMF link followed by wireless transmission. Based on the obtained results, it can be concluded that the proposed optical-fiber Kerr-shutter-based UWB doublet pulse generation scheme can be a powerful means for IR-UWB-based fiber/wireless-transmission systems.

Acknowledgments

This research work was supported by the Basic Science Research Program through the National Research Foundation of Korea (NRF) funded by the Ministry of Education, Science, and Technology (MEST), Republic of Korea (No.2010-0009799).